

# An Implicit Scheme for Solving the Convection–Diffusion–Reaction Equation in Two Dimensions

Tony W. H. Sheu, S. K. Wang, and R. K. Lin

*Department of Naval Architecture and Ocean Engineering, National Taiwan University,  
Taipei, Taiwan, Republic of China*

Received July 12, 1999; revised July 18, 2000

---

In this paper we consider a passive scalar transported in two-dimensional flow. The governing equation is that of the convection–diffusion–reaction equation. For purposes of computational efficiency, we apply an alternating-direction implicit scheme akin to that proposed by Polezhaev. Use of this implicit operator-splitting scheme allows the application of a tridiagonal Thomas solver to obtain the solution. Within each solution step, a semidiscretization scheme is applied to discretize the differential equation in one dimension. We approximate the time derivative term using a forward time-stepping scheme. The resulting inhomogeneous differential equation has only the spatial derivative terms and is solved using a newly proposed nodally exact steady-state convection–diffusion–reaction scheme. Details on the development of the flux discretization scheme are provided. Modified equation analysis, Fourier stability analysis, and a study on scheme monotonicity are also performed to shed further light on the proposed transient scheme. To validate the proposed scheme, we first consider test problems which are amenable to analytic solutions. Good agreement is obtained with both one- and two-dimensional steady/unsteady problems, thus demonstrating the validity of the method. © 2000 Academic Press

*Key Words:* two-dimensional convection–diffusion–reaction equation; nodally exact; modified equation analysis; Fourier stability analysis; monotonicity.

---

## 1. INTRODUCTION

In this paper, we investigate numerical methods for solving a convection–diffusion–reaction (CDR) scalar transport equation. This equation is practically important because the working equations of many cases fall into this category. Typical examples are the Helmholtz equation for modeling exterior acoustics [1], constitutive equations for modeling the turbulent quantities  $k$  and  $\epsilon$  [2], and viscoelastic constitutive equations for modeling the extra stresses in non-Newtonian fluid flows [3]. Furthermore, calculation of the

magnetic field  $\mathbf{B}$  using the magnetic equation  $\frac{\partial \mathbf{B}}{\partial t} = \nabla \times (\mathbf{u} \times \mathbf{B})$ , coupled with the incompressible Navier–Stokes equations, involves a convection–diffusion–reaction model equation [4]. It is this wide application scope that makes numerical prediction of this model equation worthwhile. Considerable effort has been invested in developing convection–diffusion schemes. However, comparatively few studies have been devoted to the more general convection–diffusion–reaction equation [5–11]. Some of the previous studies were focused on developing a discontinuity-capturing CDR scheme [12–14].

A reliable numerical model must have the ability to simulate transport phenomenon accurately while being able to suppress numerical instability arising in the course of discretization. The problem with numerical instability is particularly important since both advective and reactive terms may cause the solutions to diverge. It is, then, a question of constructing upwind schemes which can stabilize the finite-difference equation, and this motivated the present study. In this paper, we are also concerned with prediction accuracy since we do not regard a scheme as useful if it cannot provide accuracy to a certain high level. In addition, the lack of alignment of coordinate lines with the flow direction can result in unacceptable accuracy in the computation of two-dimensional problems. The aim of the present paper is to find a way to solve this problem.

The rest of this paper is organized as follows. Section 2 presents the working equation. In Section 3, an alternating-direction implicit scheme, similar to that of Polezhaev [15], is presented. This is followed by presentation of the semidiscretization finite-difference scheme used to solve the steady/transient CDR equation in one dimension. Our emphasis is on the derivation of a nodally exact scheme for the investigated differential equation. Section 4 is devoted to fundamental studies of the proposed flux discretization scheme, with emphasis on modified equation analysis and Fourier (or von Neumann) stability analysis. Section 5 presents numerical results that demonstrate the validity of the method. In Section 6, we give concluding remarks.

## 2. WORKING EQUATIONS AND SOLUTION ALGORITHM

We consider in this paper the finite-difference solution of the scalar convection–diffusion–reaction equation

$$\phi_t + u\phi_x + v\phi_y - k(\phi_{xx} + \phi_{yy}) + c\phi = 0, \quad (1)$$

where  $u$  and  $v$  represent the velocity components along the  $x$  and  $y$  directions, respectively. Other coefficients involve  $k$  and  $c$ , which denote the diffusion coefficient and the reaction coefficient, respectively. For illustrative purposes, all these values are assumed to be constant throughout. For simplicity, the investigated equation is subject to the Dirichlet-type boundary condition

$$\phi = g. \quad \text{on } \partial\Omega, t \in (0, T). \quad (2)$$

Equations (1) and (2) constitute a closure problem provided that the initial data of  $\phi(x, y, 0)$  are prescribed.

The strategy we will consider for solving (1) is similar to the ADI (alternating-direction implicit) scheme of Polezhaev [15]. By virtue of operator splitting, calculation of the

approximated solution of Eq. (1) is accomplished in two steps, the *predictor step*,

$$\phi^* + \frac{\Delta t}{2}(u\phi_x^* - k\phi_{xx}^*) + \frac{\Delta t}{2}c\phi^* = \phi^n - \frac{\Delta t}{2}(v\phi_y^n - k\phi_{yy}^n), \quad (3)$$

and the *corrector step*,

$$\phi^{n+1} + \frac{\Delta t}{2}(v\phi_y^{n+1} - k\phi_{yy}^{n+1}) + \frac{\Delta t}{2}c\phi^{n+1} = \phi^* - \frac{\Delta t}{2}(u\phi_x^* - k\phi_{xx}^*). \quad (4)$$

Define

$$(\bar{u}', \bar{v}') = \left( \frac{\Delta t}{2}u, \frac{\Delta t}{2}v \right), \quad (5)$$

$$\bar{k}' = \frac{\Delta t}{2}k, \quad (6)$$

$$\bar{c}' = 1 + \frac{\Delta t}{2}c. \quad (7)$$

The above two-step ADI scheme for solving Eq. (1) can be rewritten as

$$\bar{u}'\phi_x^* - \bar{k}'\phi_{xx}^* + \bar{c}'\phi^* = f_1, \quad (8)$$

$$\bar{v}'\phi_y^{n+1} - \bar{k}'\phi_{yy}^{n+1} + \bar{c}'\phi^{n+1} = f_2. \quad (9)$$

In the above, the source terms  $f_1$  and  $f_2$  are

$$f_1 = \phi^n - \bar{v}'\phi_y^n + \bar{k}'\phi_{yy}^n, \quad (10)$$

$$f_2 = \phi^* - \bar{u}'\phi_x^* + \bar{k}'\phi_{xx}^*. \quad (11)$$

For the unsteady case, the scalar convection-diffusion-reaction equation in one dimension is of the form

$$\phi_t + u\phi_x - k\phi_{xx} + c\phi = 0. \quad (12)$$

We apply the semidiscretization scheme to approximate Eq. (12). In the time-stepping scheme, we consider  $\phi_t = (\phi^{n+1} - \phi^n)/\Delta t$ , which yields first-order accuracy. The resulting equation containing only the spatial derivatives is

$$\bar{u}\phi_x^{n+1} - \bar{k}\phi_{xx}^{n+1} + \bar{c}\phi^{n+1} = \phi^n. \quad (13)$$

The definitions of  $\bar{u}$ ,  $\bar{k}$ , and  $\bar{c}$  are  $\bar{u} = u\Delta t$ ,  $\bar{k} = k\Delta t$ , and  $\bar{c} = 1 + c\Delta t$ .

### 3. FLUX DISCRETIZATION SCHEME

Equations (8), (9), and (12) are known as the steady-state convection-diffusion-reaction equations. At this point, we realize that the key to success in solving Eq. (1) lies in the analysis of the following model equation:

$$u\phi_x - k\phi_{xx} + c\phi = f. \quad (14)$$

As is the case when a partial differential equation is simulated, we aim to obtain higher

prediction accuracy. To this end, we employ the general solution for Eq. (14),

$$\phi = ae^{\lambda_1 x} + be^{\lambda_2 x} + \frac{f}{c}, \quad (15)$$

where  $a$  and  $b$  are constants. Substituting Eq. (15) into Eq. (14), we have two equations for  $\lambda_1$  and  $\lambda_2$ , respectively:

$$k\lambda_1^2 - u\lambda_1 - c = 0, \quad (16a)$$

$$k\lambda_2^2 - u\lambda_2 - c = 0. \quad (16b)$$

The above two equations enable us to determine  $\lambda_1$  and  $\lambda_2$  as follows:

$$\lambda_1 = \frac{u + \sqrt{u^2 + 4ck}}{2k}, \quad (17a)$$

$$\lambda_2 = \frac{u - \sqrt{u^2 + 4ck}}{2k}. \quad (17b)$$

For the CDR model equation (14), we can write the discrete equation at an interior node  $i$ . The idea is to approximate all the derivative terms using the center-like scheme

$$\frac{u}{2h}(\phi_{i+1} - \phi_{i-1}) - \frac{m}{h^2}(\phi_{i+1} - 2\phi_i + \phi_{i-1}) + \frac{c}{6}(\phi_{i-1} + 4\phi_i + \phi_{i+1}) = f, \quad (18a)$$

or

$$\left(-\frac{u}{2h} - \frac{m}{h^2} + \frac{c}{6}\right)\phi_{i-1} + 2\left(\frac{m}{h^2} + \frac{c}{3}\right)\phi_i + \left(\frac{u}{2h} - \frac{m}{h^2} + \frac{c}{6}\right)\phi_{i+1} = f, \quad (18b)$$

where  $h$  is the uniform grid size. Given the above discrete representation of (14), the prediction quality depends solely on  $m$  in Eq. (18). As previously noted, we seek higher accuracy through use of the exact solutions evaluated at nodal points  $x_i$  and  $x_{i\pm 1}$ . By virtue of Eq. (15), we can substitute  $\phi_i = ae^{\lambda_1 x_i} + be^{\lambda_2 x_i} + \frac{f}{c}$ ,  $\phi_{i+1} = ae^{\lambda_1 h} e^{\lambda_1 x_i} + be^{\lambda_2 h} e^{\lambda_2 x_i} + \frac{f}{c}$ , and  $\phi_{i-1} = ae^{-\lambda_1 h} e^{\lambda_1 x_i} + be^{-\lambda_2 h} e^{\lambda_2 x_i} + \frac{f}{c}$  into Eq. (18b) to derive

$$m = \frac{-(2/3)ch^2 - (ch^2/6)[\cosh(\lambda_1 h) + \cosh(\lambda_2 h)] - (uh/2)[\sinh(\lambda_1 h) + \sinh(\lambda_2 h)]}{2 - \cosh(\lambda_1 h) - \cosh(\lambda_2 h)}. \quad (19)$$

Under some extreme conditions, the values of  $\lambda_1$  and  $\lambda_2$  may lead to a zero denominator in Eq. (19). As a result, solutions cannot be obtained from Eq. (18). To avoid this situation, we can approximate Eq. (14) using another center-like scheme,

$$\frac{n}{2h}(\phi_{i+1} - \phi_{i-1}) - \frac{k}{h^2}(\phi_{i+1} - 2\phi_i + \phi_{i-1}) + \frac{c}{6}(\phi_{i-1} + 4\phi_i + \phi_{i+1}) = f, \quad (20a)$$

or

$$\left(-\frac{n}{2h} - \frac{k}{h^2} + \frac{c}{6}\right)\phi_{i-1} + 2\left(\frac{k}{h^2} + \frac{c}{3}\right)\phi_i + \left(\frac{n}{2h} - \frac{k}{h^2} + \frac{c}{6}\right)\phi_{i+1} = f. \quad (20b)$$

Substituting the general solutions for  $\phi_{i\pm 1}$  and  $\phi_i$  into Eq. (20b), we can derive  $n$  as

$$n = \frac{-(4/3)ch - 2k/h + (2k/h - ch/3)[\cosh(\lambda_1 h) + \cosh(\lambda_2 h)]}{\sinh(\lambda_1 h) + \sinh(\lambda_2 h)}. \quad (21)$$

TABLE I

A Comparison of Algebraic Expressions of Coefficients Shown in the Currently Developed Three-Point Finite-Difference Equation  $\hat{a}_i\phi_{i-1} + \hat{b}_i\phi_i + \hat{c}_i\phi_{i+1} = f$  with Those in the Exponential Fitting Scheme

	$\hat{a}_i$	$\hat{b}_i$	$\hat{c}_i$
[10]	$-\frac{u}{h} \frac{1}{\exp(-uh/k)-1}$	$-\frac{u}{h} \left[ \frac{1}{\exp(uh/k)-1} + \frac{1}{\exp(-uh/k)-1} \right] - c$	$\frac{u}{h} \frac{1}{\exp(uh/k)-1}$
Eq. (18b)	$\frac{-2c-(u/h)(e^{\lambda_1 h} + e^{\lambda_2 h} - 2)}{e^{\lambda_1 h} + e^{-\lambda_1 h} + e^{\lambda_2 h} + e^{-\lambda_2 h} - 4}$	$\frac{16c/3-(c/3)(e^{\lambda_1 h} + e^{-\lambda_1 h} + e^{\lambda_2 h} + e^{-\lambda_2 h})}{4-(e^{\lambda_1 h} + e^{-\lambda_1 h} + e^{\lambda_2 h} + e^{-\lambda_2 h})}$ $-\frac{(u/2h)(e^{\lambda_1 h} - e^{-\lambda_1 h} + e^{\lambda_2 h} - e^{-\lambda_2 h})}{4-(e^{\lambda_1 h} + e^{-\lambda_1 h} + e^{\lambda_2 h} + e^{-\lambda_2 h})}$	$\frac{-2c+(u/h)(e^{\lambda_1 h} + e^{\lambda_2 h} - 2)}{e^{\lambda_1 h} + e^{-\lambda_1 h} + e^{\lambda_2 h} + e^{-\lambda_2 h} - 4}$
Eq. (20b)	$-\frac{(2k/h^2)(e^{-\lambda_1 h} + e^{-\lambda_2 h} - 2)}{e^{\lambda_1 h} - e^{-\lambda_1 h} + e^{\lambda_2 h} - e^{-\lambda_2 h}}$ $-\frac{(c/3)(e^{\lambda_1 h} + e^{\lambda_2 h} - 4)}{e^{\lambda_1 h} - e^{-\lambda_1 h} + e^{\lambda_2 h} - e^{-\lambda_2 h}}$	$\frac{2k}{h^2} + \frac{2c}{3}$	$\frac{(2k/h^2)(e^{-\lambda_1 h} + e^{-\lambda_2 h} - 2)}{e^{\lambda_1 h} - e^{-\lambda_1 h} + e^{\lambda_2 h} - e^{-\lambda_2 h}}$ $-\frac{(c/3)(e^{\lambda_1 h} + e^{\lambda_2 h} - 4)}{e^{\lambda_1 h} - e^{-\lambda_1 h} + e^{\lambda_2 h} - e^{-\lambda_2 h}}$

As Eqs. (19) and (20) show, the coefficients shown in the proposed three-point finite-difference Eqs. (18) and (20) are functions of exponential terms. This fact provides impetus to compare with the exponential fitting scheme [10, 11], which was originally developed to solve the singularly perturbed ordinary differential equation (ODE) (14) in the case of  $k \ll 1$ . The novelty of this model development is that the second-order ODE has been exactly split into two first-order ordinary differential equations. One of them is approximated using the symmetric discretization and the other equation is approximated using the exponential fitting scheme to render a three-point scheme  $\hat{a}_i\phi_{i-1} + \hat{b}_i\phi_i + \hat{c}_i\phi_{i+1} = f$ . The reader can refer to [10] for additional details. For comparative purposes, we tabulate  $\hat{a}_i$ ,  $\hat{b}_i$ , and  $\hat{c}_i$  in Table I for the currently proposed scheme and the exponential fitting scheme [10]. While the algebraic expressions of  $\hat{a}_i$ ,  $\hat{b}_i$ , and  $\hat{c}_i$  are quite different, their values, tabulated in Table II, are identical for the case with  $u = 1, k = -1, c = -2$ , and  $h (= \frac{1}{20}$  and  $\frac{1}{100})$ .

TABLE II

A Comparison of Values of Coefficients Shown in the Currently Developed Three-Point Finite-Difference Equation  $\hat{a}_i\phi_{i-1} + \hat{b}_i\phi_i + \hat{c}_i\phi_{i+1} = f$  with Those in the Exponential Fitting Scheme

	$\hat{a}_i$		$\hat{b}_i$		$\hat{c}_i$	
	$h = \frac{1}{20}$	$h = \frac{1}{100}$	$h = \frac{1}{20}$	$h = \frac{1}{100}$	$h = \frac{1}{20}$	$h = \frac{1}{100}$
(a) $u = 1, k = -1, c = -2$						
Ref. [10]	390.0833	9950.0833	802.1666	20002.1666	410.0833	10050.0833
Eq. (18b)	389.9500	9949.9500	801.9001	20001.9000	409.9500	10049.9500
Eq. (20b)	389.7020	9949.6737	801.3333	20001.3333	409.6313	10049.6595
(b) $u = 1, k = 1, c = 1$						
Ref. [10]	-410.0833	-10050.0833	801.1666	20001.1666	-390.0833	-9950.0833
Eq. (18b)	-410.0277	-10050.0277	801.0555	20001.0555	-390.0277	-9950.0277
Eq. (20b)	-409.8187	-10049.8304	800.6666	20000.6666	-389.8479	-9949.8362
(c) $u = 1, k = x, c = -1$						
Ref. [10]	-70.5545	-1550.5555	120.1090	3000.1111	-50.5545	-1450.5555
Eq. (18b)	-70.5191	-1550.5198	120.0382	3000.0397	-50.5191	-1450.5198
Eq. (20b)	-70.1257	-1550.1584	119.3333	2999.3334	-50.2076	-1450.1749

After developing the discretization scheme for the CDR model equation, we proceed with the calculation of  $\phi^{n+1}$  from Eqs. (8) and (9) as follows. First we compute the source term  $f_1$  using the previous solutions computed at  $t = n\Delta t$ . This is followed by computing the solution  $\phi^*$  using the nodally exact CDR scheme (18) or (20). Upon obtaining the value of  $\phi^*$ , we can compute  $f_2$  and then the solution  $\phi^{n+1}$  using the same nodally exact CDR scheme used in the predictor step.

#### 4. FUNDAMENTAL STUDY OF THE DISCRETIZATION SCHEME

To shed light on the nature of the proposed convection–diffusion–reaction scheme, we will conduct a modified equation analysis [16]. The scheme given in (18) is considered for illustration. Using the scheme derived in Section 3, we can write the discretization equation for Eq. (13) as

$$\frac{\bar{u}}{2h}(\phi_{i+1}^{n+1} - \phi_{i-1}^{n+1}) - \frac{\bar{m}}{h^2}(\phi_{i+1}^{n+1} - 2\phi_i^{n+1} + \phi_{i-1}^{n+1}) + \frac{\bar{c}}{6}(\phi_{i-1}^{n+1} + 4\phi_i^{n+1} + \phi_{i+1}^{n+1}) = \phi_i^n. \quad (22)$$

The expression for  $\bar{m}$  is similar to  $m$ , defined in (19),

$$\bar{m} = \frac{-(2/3)\bar{c}h^2 - (\bar{c}h^2/6)[\cosh(\bar{\lambda}_1 h) + \cosh(\bar{\lambda}_2 h)] - (\bar{u}h/2)[\sinh(\bar{\lambda}_1 h) + \sinh(\bar{\lambda}_2 h)]}{2 - \cosh(\bar{\lambda}_1 h) - \cosh(\bar{\lambda}_2 h)}, \quad (23)$$

where

$$\bar{\lambda}_1 = \frac{\bar{u} + \sqrt{\bar{u}^2 + 4\bar{c}\bar{k}}}{2\bar{k}}, \quad (24)$$

$$\bar{\lambda}_2 = \frac{\bar{u} - \sqrt{\bar{u}^2 + 4\bar{c}\bar{k}}}{2\bar{k}}. \quad (25)$$

Substituting Taylor-series expansions into Eq. (22) for  $\phi_{i+1}^{n+1}$ ,  $\phi_{i-1}^{n+1}$ ,  $\phi_i^{n+1}$ , and  $\phi_i^n$ , we obtain

$$\begin{aligned} \phi_t + u\phi_x - k\phi_{xx} + c\phi = & -u \left[ (\Delta t)\phi_{xx} + \frac{(\Delta t)^2}{2}\phi_{ttx} + \frac{h^2}{6}\phi_{xxx} \right] - k\phi_{xx} \\ & + \frac{\bar{m}}{\Delta t} \left[ \phi_{xx} + \frac{h^2}{6(\Delta t)}\phi_{txx} + \frac{(\Delta t)^2}{6}\phi_{ttxx} \right] \\ & - \left[ \frac{\Delta t}{2}\phi_{tt} + \frac{h^2}{6(\Delta t)}\phi_{xx} + \frac{(\Delta t)^2}{6}\phi_{ttt} + \frac{h^2}{6}\phi_{txx} \right] \\ & - c \left[ (\Delta t)\phi_t + \frac{(\Delta t)^2}{2}\phi_{tt} + \frac{h^2}{6}\phi_{xx} \right] + O[(\Delta t)^3, h^3]. \quad (26) \end{aligned}$$

Note that the left-hand side of Eq. (26) is the investigated model equation while the right-hand side represents the discretization error that may be produced. The significance of the terms on the right-hand side is easily seen if the time derivatives are replaced with spatial derivative terms. As a result, the modified equation for Eq. (12) is derived

as

$$\begin{aligned}
 \phi_t + u\phi_x - k\phi_{xx} + c\phi = & \left\{ \frac{c^2}{2}\Delta t - \frac{c^3}{3}(\Delta t)^2 + O[(\Delta t)^3] \right\} \phi \\
 & + \{cu\Delta t - c^2u(\Delta t)^2 + O[(\Delta t)^3]\} \phi_x \\
 & + \left\{ -k + \frac{\bar{m}'}{\Delta t} - c\bar{m}' + \frac{c\bar{m}'}{2}\Delta t + \frac{u^2}{2}\Delta t \right. \\
 & \left. + \left( \frac{1}{2}c^2k - cu^2 \right) (\Delta t)^2 + O[(\Delta t)^3, h^3] \right\} \phi_{xx} + \dots \quad (27)
 \end{aligned}$$

where

$$\bar{m}' = \bar{m} - \frac{\bar{c}}{6}h^2 = \frac{\bar{c}h^2 + (\bar{u}h/2)[\sinh(\bar{\lambda}_1h) + \sinh(\bar{\lambda}_2h)]}{[\cosh(\bar{\lambda}_1h) + \cosh(\bar{\lambda}_2h)] - 2}. \quad (28)$$

For a finite value of  $\Delta t$ , the following limiting condition holds:

$$\lim_{h \rightarrow 0} \bar{m}' = k\Delta t. \quad (29)$$

From Eq. (27), it is clear that the consistency property necessary to obtain a convergent solution is satisfied as  $\Delta t$  and  $h$  both approach zero.

As a fundamental study of the proposed scheme, we will also consider Fourier (or von Neumann) stability analysis. First, we can derive the amplification factor for this scheme by conducting standard stability analysis. Let  $\beta = \frac{2\pi m}{2L}h$  ( $m = 0, 1, 2, 3, \dots, M$ ), let  $h$  be the grid size, and let  $2L$  be the period of the fundamental frequency ( $m = 1$ ); the amplification factor  $|G|$  ( $\equiv |\phi_j^{n+1}/\phi_j^n|$ ) is derived as

$$G = \frac{A - iB}{A^2 + B^2}, \quad (30a)$$

$$|G| = \frac{1}{\sqrt{A^2 + B^2}}, \quad (30b)$$

where

$$A = \bar{c} + \frac{(1 - \cos \beta)\{\bar{c} + (\bar{u}/k) \sinh(\bar{u}/2\bar{k}) \cosh(\sqrt{\bar{u}^2 + 4\bar{c}\bar{k}}/2\bar{k})\}}{\cosh(\bar{u}/2\bar{k}) \cosh(\sqrt{\bar{u}^2 + 4\bar{c}\bar{k}}/2\bar{k}) - 1}, \quad (31a)$$

$$B = \frac{\bar{u}}{\bar{k}} \sin \beta. \quad (31b)$$

Referring to Appendix 1, we see that  $|G| \leq 1$ . Therefore, the scheme proposed here is unconditionally stable.

The amplification factor shown in (30a) can be rewritten in its exponential form  $G = |G|e^{i\theta}$ , where  $\theta$  is the phase angle,

$$\theta = \tan^{-1} \left| \frac{\text{Im}(G)}{\text{Re}(G)} \right| = \tan^{-1} \left( \frac{-B}{A} \right). \quad (32)$$

To study how this phase varies with the dimensionless numbers

$$R_1 = \frac{ch^2}{2k}, \quad (33a)$$

$$R_2 = \frac{ch}{u}, \quad (33b)$$

$$R_3 = \frac{R_1}{R_2} = \frac{uh}{2k}, \quad (33c)$$

$$\nu = \frac{u \Delta t}{h}, \quad (33d)$$

we must derive the exact phase angle  $\theta_c$ . The detailed derivation is given in Appendix 2. Upon deriving the exact phase angle, we can obtain the relative phase shift error over an arbitrary time step as

$$\frac{\theta}{\theta_c} = \frac{\tan^{-1}(-B/A)}{-\nu\beta}. \quad (34)$$

We plot  $\frac{\theta}{\theta_c}$  against  $\beta$ ,  $R_1$ ,  $R_2$ , and  $\nu$  in Fig. 1. When the relative phase error exceeds 1 for the specified values of  $R_1$  and  $R_2$ , the numerical solution has a wave speed greater than the exact wave speed, and this is called the phase-leading error. The converse error is called a phase-lagging error. As the figure shows, the proposed scheme has a phase-lagging error irrespective of  $R_1$ ,  $R_2$ , and  $\nu$ . Therefore, the implicit scheme proposed in this paper is called a phase-lagging finite-difference scheme.

Observations revealed by Fig. 1 are summarized below. As Figs. 1a and 1b, which plot  $\frac{\theta}{\theta_c}$  against  $R_1$  at the fixed values of  $\nu = 1$  and  $R_2 = 0.001$ , show, the value of  $\frac{\theta}{\theta_c}$  increases with increased  $R_1$ . This gives an indication that the higher  $R_3$  is, the less accurate is the phase predicted under the circumstances. At the fixed values of  $\nu = 1$  and  $R_1 = 0.001$ , Fig. 1b plots  $\frac{\theta}{\theta_c}$  against  $R_2$ . As Fig. 1b shows, when the reaction term becomes increasingly dominant over the convection term, the numerical phase continuously departs from the exact phase. For the purpose of comparison, we also plot  $\frac{\theta}{\theta_c}$  against  $R_1$  at  $\nu = 0.2$ ,  $R_2 = 0.001$  in Fig. 1c and against  $R_2$  at  $\nu = 0.2$ ,  $R_1 = 0.001$  in Fig. 1d. As Figs. 1a–d show, even

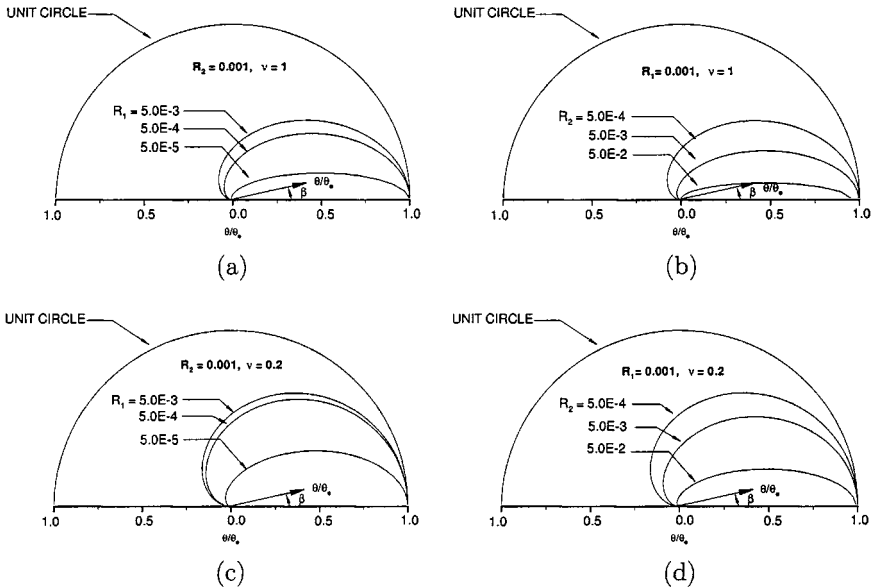


**FIG. 1.** Plots of  $\frac{\theta}{\theta_c}$  against  $R_1$ ,  $R_2$ , and  $\nu$ . (a)  $R_2 = 0.001$ ,  $\nu = 1$ ; (b)  $R_1 = 0.001$ ,  $\nu = 1$ ; (c)  $R_2 = 0.001$ ,  $\nu = 0.2$ ; (d)  $R_1 = 0.001$ ,  $\nu = 0.2$ .

the proposed scheme is unconditionally stable; the increase of the chosen time step, which corresponds to increasing  $\nu$ , will deteriorate the phase prediction.

Inspection of the banded tridiagonal matrix Eqs. (18b) and (20b) shows that it is possible to have  $a_{ij} \leq 0$  with  $i \neq j$  and  $|a_{ii}| \geq \sum |a_{ij}|$  ( $i \leq j$ ). If this is the case, the matrix equation is, by definition, considered to be irreducible diagonally dominant. A matrix of this type is called an  $M$ -matrix, and  $\underline{\underline{A}}^{-1} > 0$  holds. Under this condition, the solutions computed from the  $M$ -matrix equation are unconditionally monotonic. By virtue of the  $M$ -matrix theory [17], there is a potential advantage in using the proposed scheme to resolve any possible sharp gradient in the flow. We will address this issue through examples considered in Section 5.2.2.

## 5. NUMERICAL RESULTS

### 5.1. One-Dimensional Problems

As is the case when a new scheme for solving any differential equation is presented, we have to validate the proposed scheme. For this purpose, we will employ test problems which are amenable to analytic solutions.

*5.1.1. Homogeneous CDR equation.* For Eq. (14), we consider first the homogeneous case where  $f = 0$ . To keep matters simple, coefficients  $u$ ,  $k$ , and  $c$  are all assumed to be constant in the region  $0 \leq x \leq 1$ . Under the assumption that  $k = -1$ ,  $u = 1$ , and  $c = -2$ , the exact solution for (14) takes the form

$$\phi_{\text{exact}} = e^x + e^{-2x}. \quad (35)$$

This solution is obtained under uniform grid size ( $h = \frac{1}{20}$ ) and the boundary conditions  $\phi(x = 0) = 2$  and  $\phi(x = 1) = (1 + e^3)/e^2$ . The computed result, shown in Fig. 2, is found to reproduce the analytic solution of the test equation. This test verifies that the proposed finite-difference scheme can provide a nodally exact steady-state solution.

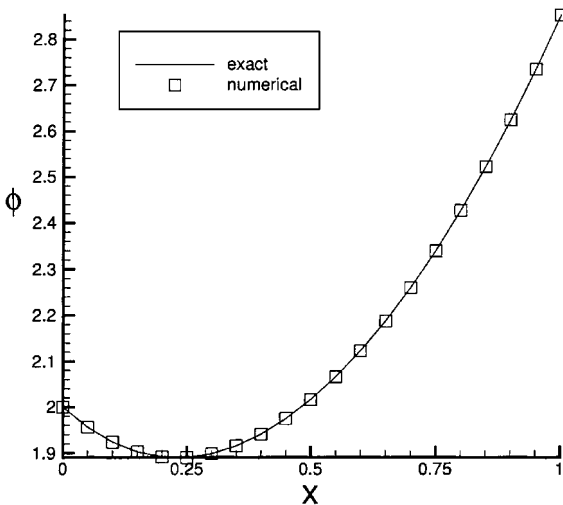


**FIG. 2.** A comparison of exact and numerical solutions for the one-dimensional steady homogeneous CDR equation considered in Section 5.1.1.

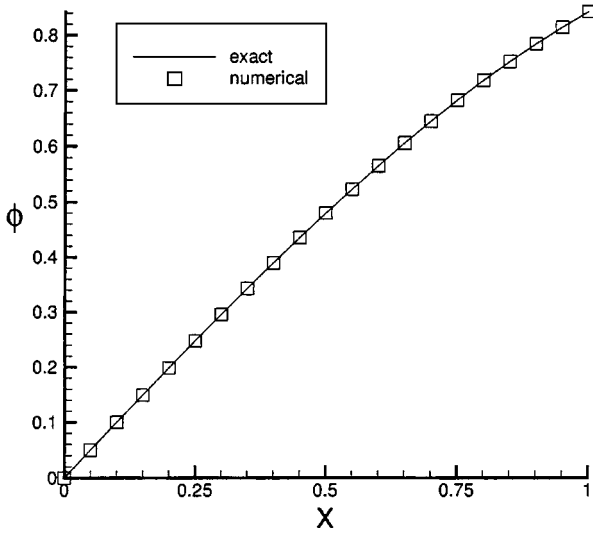


**FIG. 3.** A comparison of exact and numerical solutions for the one-dimensional steady inhomogeneous CDR equation considered in Section 5.1.2.

*5.1.2. Inhomogeneous CDR equation.* Having validated the code against the above one-dimensional test problem, we now draw our attention to the inhomogeneous case where  $f = \cos x - 3 \sin x$ . To allow comparison with the analytic solution, we consider a second test problem which involves constant coefficients:  $k = -1$ ,  $u = 1$ ,  $c = -2$ . Subject to Dirichlet-type boundary condition, the exact solution to the inhomogeneous convection–diffusion–reaction equation is derived as

$$\phi_{\text{exact}} = \sin x. \quad (36)$$

Uniform grids are overlaid on the region  $0 \leq x \leq 1$ . The results plotted in Fig. 3 show good agreement with the exact solutions, thus demonstrating the applicability of the proposed scheme to solving the inhomogeneous CDR equation.

To further verify that the scheme is applicable to problems containing discontinuous source terms, we will consider the case where

$$f = \begin{cases} 0, & x < \frac{1}{2} \\ 8 \times 10^3, & x \geq \frac{1}{2}. \end{cases} \quad (37)$$

Subject to the boundary conditions  $\phi(x = 0) = 0$  and  $\phi(x = 1) = 1$ , the exact solution takes the form

$$\phi = \begin{cases} \frac{1}{2} \frac{\sinh(\lambda x)}{\sinh(\lambda/2)}, & x \leq \frac{1}{2} \\ 1 - \frac{1}{2} \frac{\sinh(\lambda(1-x))}{\sinh(\lambda/2)}, & x \geq \frac{1}{2}, \end{cases} \quad (38)$$

where  $\lambda = (c/k)^{1/2}$ . In this case we will consider  $k = 1$ ,  $u = 0$ ,  $c = 8 \times 10^3$ , and  $h = \frac{1}{20}$ . Figure 4 shows the exact solution (solid line) and the numerical solution (square symbols). Good agreement between the two sets of solutions is obtained.

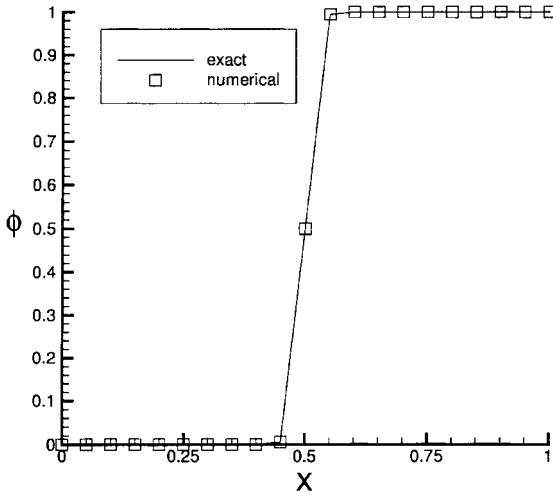


FIG. 4. A comparison of exact and numerical solutions for the one-dimensional CDR equation with a discontinuous source term considered in Section 5.1.3.

5.1.3. *Unsteady inhomogeneous CDR equation.* Having verified the proposed steady-state scheme, we now turn our attention to the transient convection–diffusion–reaction equation in a unit domain of  $0 \leq x \leq 1$ ,

$$\phi_t + u\phi_x - k\phi_{xx} + c\phi = f, \quad (39)$$

where  $f = 2(x - 1)e^{-t}$ . We start the calculation with the initial data  $\phi(x, t = 0) = x^2$ . The exact solution for the case with  $u = 1$ ,  $c = 1$ , and  $k = 1$  takes the form

$$\phi_{\text{exact}}(x, t) = x^2 e^{-t}. \quad (40)$$

Under the time step  $\Delta t = 5 \times 10^{-2}$ , the computed solution agrees well with the exact solution plotted in Fig. 5. We also carried out computations on continuously refined grids,

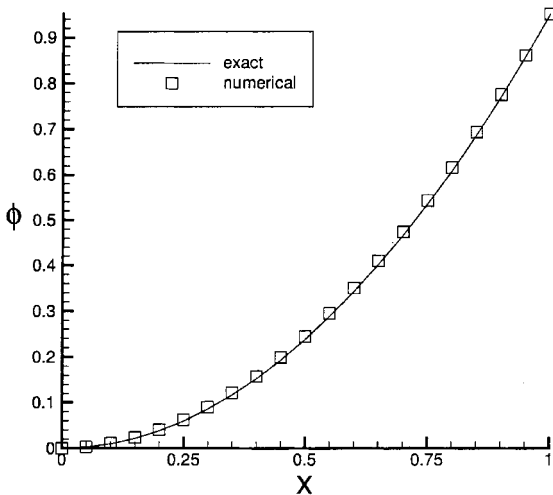
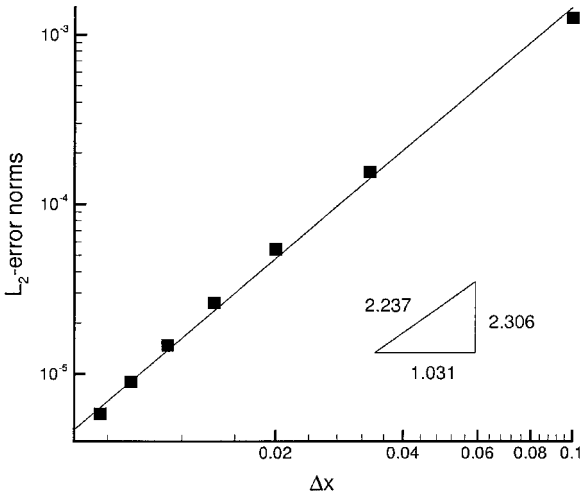


FIG. 5. A comparison of numerical and exact solutions for the one-dimensional time-dependent inhomogeneous CDR equation considered in Section 5.1.4.



**FIG. 6.** The rate of convergence plot for the inhomogeneous time-dependent CDR equation considered in Section 5.1.4.

namely  $h = \frac{1}{10}, \frac{1}{20}, \frac{1}{40}, \frac{1}{80},$  and  $\frac{1}{100}$ , and cast prediction errors in their  $L_2$ -norms. This was followed by plotting  $\log(\text{err}_1/\text{err}_2)$  against  $\log(h_1/h_2)$  for the errors  $\text{err}_1$  and  $\text{err}_2$  computed at two continuously refined grids  $h_1$  and  $h_2$ . As Fig. 6 shows, the rate of convergence is obtained as 2.237 using the proposed scheme.

### 5.2. Two-Dimensional Problems

*5.2.1. Analytical validation.* Simulations were also performed in the two-dimensional domain. In this paper, we will first present a simple test case to justify the use of the proposed ADI scheme to simulate Eq. (1) in the square  $0 \leq x, y \leq \pi$ . This test problem was considered by Yu [18]:

$$\phi_{xx} + \phi_{yy} + \phi = 0. \tag{41}$$

Provided that the Dirichlet-type boundary condition for  $\phi$  is analytically specified, this equation is amenable to the exact solution

$$\begin{aligned} \phi = \cos y - \frac{\sqrt{2}}{2} \sin\left(\frac{\pi}{4} + y\right) & \left[ C\left(\sqrt{\frac{2(\rho - y)}{\pi}}\right) + S\left(\sqrt{\frac{2(\rho + y)}{\pi}}\right) \right] \\ & - \frac{\sqrt{2}}{2} \sin\left(\frac{\pi}{4} - y\right) \left[ C\left(\sqrt{\frac{2(\rho + y)}{\pi}}\right) + S\left(\sqrt{\frac{2(\rho - y)}{\pi}}\right) \right], \end{aligned} \tag{42}$$

where  $\rho = (x^2 + y^2)^{1/2}$ . In Eq. (42),  $C(p)$  and  $S(q)$  denote the sine Eresnel integral and cosine Fresnel integral, respectively; i.e.,

$$C(p) \equiv \sqrt{\frac{2}{\pi}} \int_0^p \cos u^2 du \approx \sqrt{\frac{2}{\pi}} \left( p - \frac{p^5}{5 \cdot 2!} + \frac{p^9}{9 \cdot 4!} - \frac{p^{13}}{13 \cdot 6!} + \dots \right), \tag{43a}$$

$$S(q) \equiv \sqrt{\frac{2}{\pi}} \int_0^q \sin u^2 du \approx \sqrt{\frac{2}{\pi}} \left( \frac{q^3}{3} - \frac{q^7}{7 \cdot 3!} + \frac{q^{11}}{11 \cdot 5!} - \frac{q^{15}}{15 \cdot 7!} + \dots \right). \tag{43b}$$

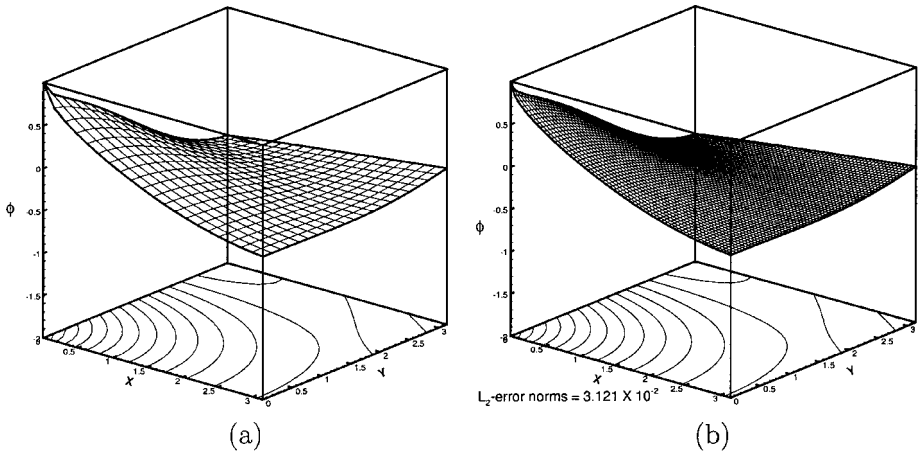


**FIG. 7.** The contour plots of  $\phi$  for Eq. (41) considered in Section 5.2.1. (a) Exact contours computed from Eq. (42). (b) Computed contours of  $\phi$  and the  $L_2$ -error norm for the case with  $\Delta x = \Delta y = \frac{1}{60}$ .

We computed solutions on two-dimensional grids with a uniform resolution of  $\Delta x = \Delta y = \frac{1}{60}$  and plotted  $\phi$  in their contour-valued format. As Fig. 7 shows, good agreement with the analytic solution is obtained. The computed  $L_2$ -error norm is also shown in Fig. 7.

*5.2.2. Test problem proposed by Codina.* Having verified the applicability of the proposed scheme in solving the two-dimensional smooth problem, we now consider a more stringent test case. In all the test cases, the source term was taken as  $f = 1$ , and the diffusion coefficient was set to  $k = 10^{-4}$ . For simplicity, the velocity vector  $\mathbf{u}$  was assumed to be constant and was taken as  $(u = |\bar{u}| \cos(\frac{\pi}{3}), v = |\bar{u}| \sin(\frac{\pi}{3}))$ . Three cases considered by Codina [14] are investigated here:

$$|\bar{u}| = 1, \quad c = 10^{-4}; \tag{44a}$$

$$|\bar{u}| = 10^{-4}, \quad c = 1; \tag{44b}$$

$$|\bar{u}| = 0.5, \quad c = 1. \tag{44c}$$

All three test cases, detailed in Tables III and IV, were subject to the homogeneous Dirichlet-type boundary condition  $\phi(\bar{x} \in \partial\Omega)$ . Simulations were performed on uniform

**TABLE III**  
**Details of the Problem Considered in Section 5.2.2**

Problems	Eq. (44a)	Eq. (44b)	Eq. (44c)
$k$	$10^{-4}$	$10^{-4}$	$10^{-4}$
$u$	1	$10^{-4}$	0.5
$c$	$10^{-4}$	1	1
$f$	1	1	1
$\lambda_1$	$10^4$	$10^2$	$0.502 \times 10^4$
$\lambda_2$	$-10^{-4}$	$-10^{-2}$	$1.922 \times 10$
$m$	$\frac{ch^2}{6} + \frac{uh}{2}$	$10^{-4}$	$10^{-4}$
$n$	$10^{-4}$	$-\frac{2k}{h} + \frac{ch}{3}$	$\frac{2k}{h} - \frac{uh}{3}$

**TABLE IV**  
**Computational Details for the Problem Considered in Section 5.2.2**

	Eq. (44a)	Eq. (44b)	Eq. (44c)
$h = \frac{1}{20}$			
$R_1 = \frac{ch^2}{2k}$	$1.25 \times 10^{-3}$	$1.25 \times 10$	$1.25 \times 10$
$R_2 = \frac{ch}{u}$	$5.0 \times 10^{-6}$	$5.0 \times 10^{-6}$	0.1
$R_3 = \frac{R_1}{R_2} = \frac{uh}{2k}$	$0.25 \times 10^3$	$0.25 \times 10^{-1}$	$0.25 \times 10^2$
$h = \frac{1}{52}$			
$R_1 = \frac{ch^2}{2k}$	$1.85 \times 10^{-4}$	1.85	1.85
$R_2 = \frac{ch}{u}$	$1.92 \times 10^{-6}$	$1.92 \times 10^2$	$0.38 \times 10^{-1}$
$R_3 = \frac{R_1}{R_2} = \frac{uh}{2k}$	$0.96 \times 10^3$	$0.96 \times 10^{-2}$	$0.48 \times 10^2$
$h = \frac{1}{100}$			
$R_1 = \frac{ch^2}{2k}$	$0.5 \times 10^{-4}$	0.5	0.5
$R_2 = \frac{ch}{u}$	$10^{-8}$	1	$0.5 \times 10^{-3}$
$R_3 = \frac{R_1}{R_2} = \frac{uh}{2k}$	$0.5 \times 10^4$	0.5	$10^3$

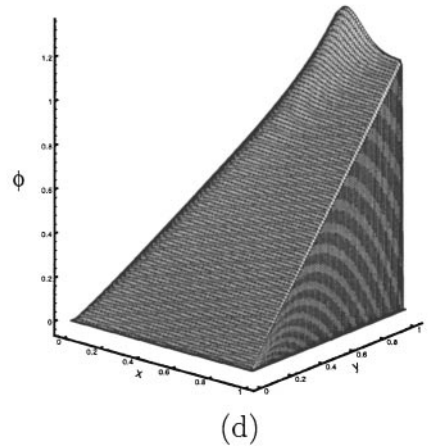
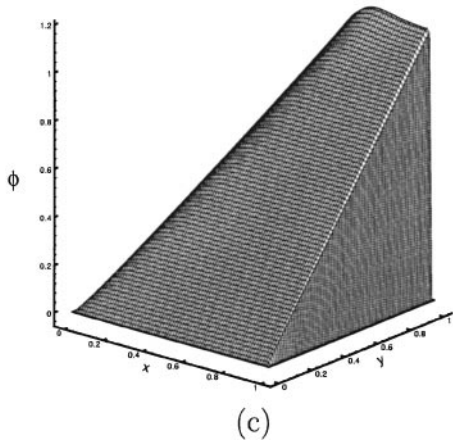
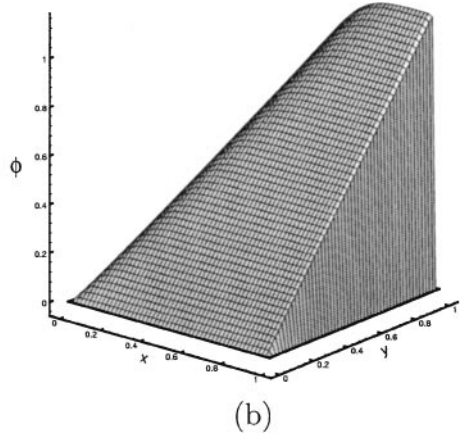
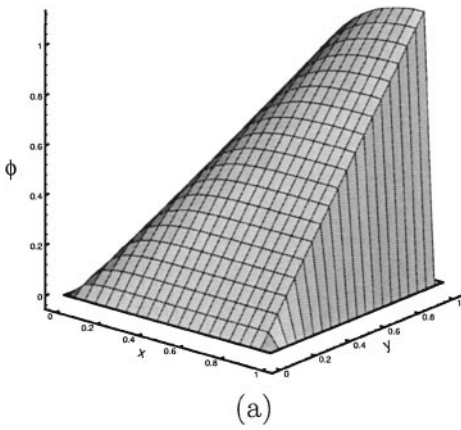


**FIG. 8.** Computed solutions of  $\phi$  for the case given in (44a). (a)  $\Delta x = \Delta y = \frac{1}{20}$ ; (b)  $\Delta x = \Delta y = \frac{1}{52}$ ; (c)  $\Delta x = \Delta y = \frac{1}{80}$ ; (d)  $\Delta x = \Delta y = \frac{1}{100}$ .

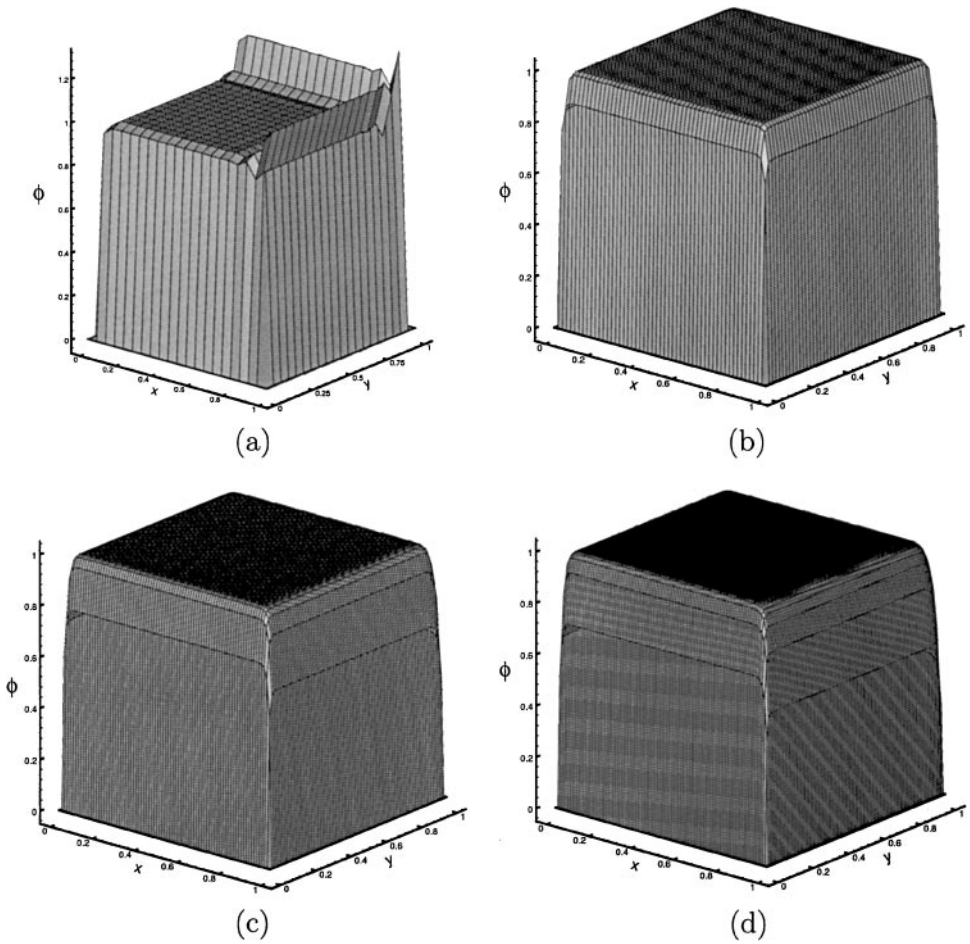


**FIG. 9.** Computed solutions of  $\phi$  for the case given in (44b). (a)  $\Delta x = \Delta y = \frac{1}{20}$ ; (b)  $\Delta x = \Delta y = \frac{1}{52}$ ; (c)  $\Delta x = \Delta y = \frac{1}{80}$ ; (d)  $\Delta x = \Delta y = \frac{1}{100}$ .

grids with different resolutions of  $\Delta x = \Delta y = \frac{1}{20}$ ,  $\frac{1}{52}$ ,  $\frac{1}{80}$ , and  $\frac{1}{100}$ . In these tests, solutions were obtained as the residuals, cast in the  $L_2$ -norm, computed between  $x$ - and  $y$ -sweeps fell below  $10^{-9}$ . The resulting steady-state solutions for the three test conditions are plotted in Figs. 8–10, respectively. As these figures reveal, sharp profiles of  $\phi$  could be captured without postshock oscillations. These tests demonstrate that the discretization scheme exhibits strong stability even in the two-dimensional domain.

While solutions for three test cases considered in Eqs. (44a)–(44c) are all monotonically predicted, this does not mean that the proposed two-dimensional finite-difference scheme always provides monotonic solutions. This is because the matrix equation involved in the implicit scheme is conditionally classified as an  $M$ -matrix. To show this, we can consider an even more severe problem with  $|\bar{u}| = 10^{-4}$ ,  $c = 1$ ,  $k = 10^{-6}$ . As Fig. 11 shows, an oscillatory solution profile is seen in regions adjacent to the boundary even when the grid size has been reduced to  $\Delta x = \Delta y = \frac{1}{80}$ . This highlights the fact that the matrix equation is not classified as an  $M$ -matrix for the investigated case and, thus, solutions may show

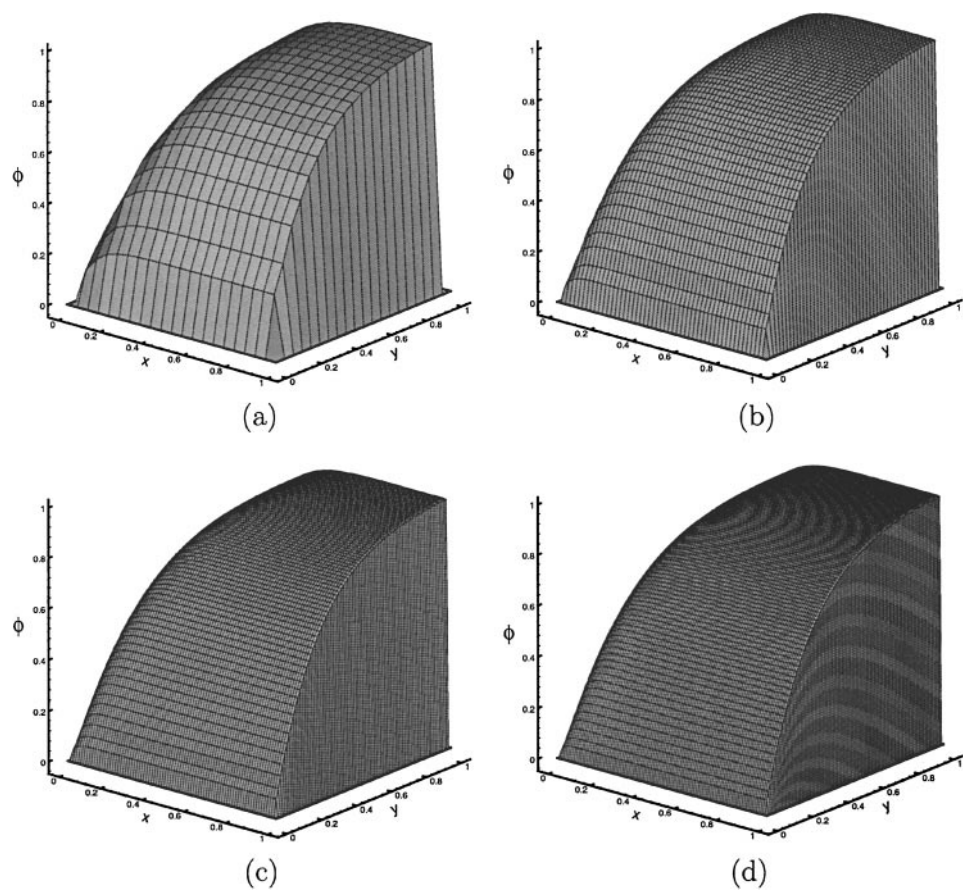


**FIG. 10.** Computed solutions of  $\phi$  for the case given in (44c). (a)  $\Delta x = \Delta y = \frac{1}{20}$ ; (b)  $\Delta x = \Delta y = \frac{1}{32}$ ; (c)  $\Delta x = \Delta y = \frac{1}{80}$ ; (d)  $\Delta x = \Delta y = \frac{1}{100}$ .

oscillations in high-gradient regions. This is not the case for conditions considered in (44a) and (44c). Even when the value of  $k$  is decreased to  $10^{-6}$ , the matrix equations for the two cases considered are all  $M$ -matrices. The solutions shown in Figs. 12 and 13 are of the monotonic type.

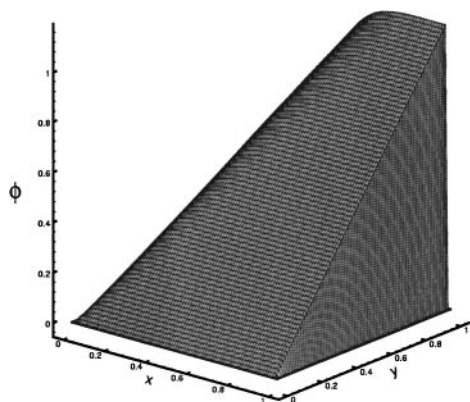


**FIG. 11.** Solution of  $\phi$  computed under  $\Delta x = \Delta y = \frac{1}{80}$  for the case with  $|\mathbf{u}| = 1$ ,  $c = 10^{-4}$ , and  $k = 10^{-6}$ .

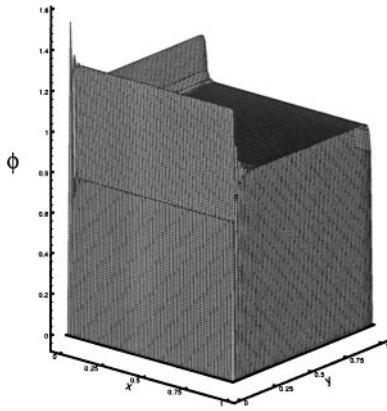


**FIG. 12.** Solution of  $\phi$  computed under  $\Delta x = \Delta y = \frac{1}{30}$  for the case with  $|\mathbf{u}| = 10^{-4}$ ,  $c = 1$ , and  $k = 10^{-6}$ .

## 6. CONCLUDING REMARKS

We have presented in this paper a finite-difference scheme for solving the two-dimensional convection–diffusion–reaction equation. To gain computational efficiency in solving the matrix equation, we have considered the alternating-direction implicit scheme, which is similar to Polezhaev’s scheme. For the sake of accuracy, we have developed a nodally exact one-dimensional convection–diffusion–reaction discretization scheme. To elucidate the nature of the proposed scheme, we have performed a fundamental study, with an emphasis on modified equation analysis and on Fourier stability analysis. We have also extended the applicability of this scheme to transient analyses by adopting the semidiscretization approach. The flux discretization scheme has been validated extensively against test cases by reproducing analytic solutions for the investigated one-dimensional equation. The application scope has also been extended to the two-dimensional problem with an exact solution. Good agreement with the smoothly varying exact solutions has been obtained, thus verifying the applicability of the proposed ADI finite-difference scheme. Also, computations have been performed for a problem with high-gradient solutions. A good ability to capture the sharply varying profiles has been demonstrated.

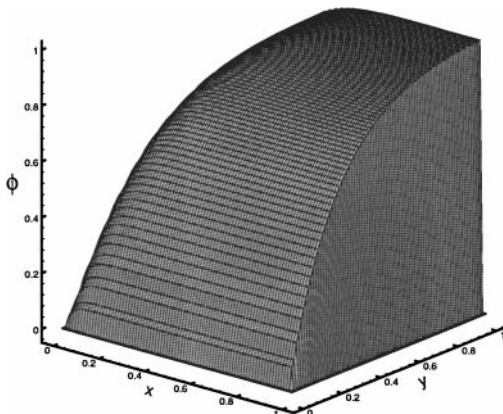


**FIG. 13.** Solution of  $\phi$  computed under  $\Delta x = \Delta y = \frac{1}{30}$  for the case with  $|\mathbf{u}| = 0.5$ ,  $c = 1$ , and  $k = 10^{-6}$ .

## APPENDIX 1

Proof of  $|G| \leq 1$ 

Recall that the modulus of the amplification factor  $|G|$  given in Eq. (30b) is derived as

$$|G| = \frac{1}{\sqrt{A^2 + B^2}}, \quad (\text{A1.1})$$

where

$$A = \bar{c} + \frac{(1 - \cos \beta)\{\bar{c} + (\bar{u}/\bar{k}) \sinh(\bar{u}/2\bar{k}) \cosh(\sqrt{\bar{u}^2 + 4\bar{c}\bar{k}}/2\bar{k})\}}{\cosh(\bar{u}/2\bar{k}) \cosh(\sqrt{\bar{u}^2 + 4\bar{c}\bar{k}}/2\bar{k}) - 1}, \quad (\text{A1.2})$$

$$B = \frac{\bar{u}}{\bar{k}} \sin \beta. \quad (\text{A1.3})$$

The above expression is derived under the condition that  $k$  and  $c$  have the same sign. Here, we take the positive sign as an example in the proof; i.e.,  $k > 0$  and  $c > 0$ . As a result, one can obtain

$$\bar{c} = 1 + c(\Delta t) > 1, \quad (\text{A1.4})$$

$$\bar{k} = k(\Delta t) > 0, \quad (\text{A1.5})$$

$$\bar{u} = u(\Delta t). \quad (\text{A1.6})$$

Given that  $\cosh(x) > 1$  for all real  $x$  (except at  $x = 0$ ), we have

$$\cosh(\bar{u}/2\bar{k}) > 1, \quad \cosh(\sqrt{\bar{u}^2 + 4\bar{c}\bar{k}}/2\bar{k}) > 1. \quad (\text{A1.7})$$

These, in turn, give

$$\cosh(\bar{u}/2\bar{k}) \cosh(\sqrt{\bar{u}^2 + 4\bar{c}\bar{k}}/2\bar{k}) - 1 > 0. \quad (\text{A1.8})$$

Since  $x \sinh x \geq 0$  for all real  $x$  and  $\bar{k} > 0$ , we have  $\frac{\bar{u}}{\bar{k}} \sinh(\frac{\bar{u}}{2\bar{k}}) \geq 0$  and, thus,

$$\left[ \bar{c} + \frac{\bar{u}}{\bar{k}} \sinh\left(\frac{\bar{u}}{2\bar{k}}\right) \cosh\left(\frac{\sqrt{\bar{u}^2 + 4\bar{c}\bar{k}}}{2\bar{k}}\right) \right] \geq 1. \quad (\text{A1.9})$$

Since  $-1 \leq \cos \beta \leq 1$ , the following equation holds by virtue of Eqs. (A1.7)–(A1.9):

$$\frac{(1 - \cos \beta)\{\bar{c} + (\bar{u}/\bar{k}) \sinh(\bar{u}/2\bar{k}) \cosh(\sqrt{\bar{u}^2 + 4\bar{c}\bar{k}}/2\bar{k})\}}{\cosh(\bar{u}/2\bar{k}) \cosh(\sqrt{\bar{u}^2 + 4\bar{c}\bar{k}}/2\bar{k}) - 1} \geq 0. \quad (\text{A1.10})$$

As a result,

$$A = \bar{c} + \frac{(1 - \cos \beta)\{\bar{c} + (\bar{u}/\bar{k}) \sinh(\bar{u}/2\bar{k}) \cosh(\sqrt{\bar{u}^2 + 4\bar{c}\bar{k}}/2\bar{k})\}}{\cosh(\bar{u}/2\bar{k}) \cosh(\sqrt{\bar{u}^2 + 4\bar{c}\bar{k}}/2\bar{k}) - 1} \geq \bar{c} > 1. \quad (\text{A1.11})$$

Since  $A^2 > 1$  and  $B^2 \geq 0$ , we have  $\sqrt{A^2 + B^2} > 1$  and, thus,  $|G| = 1/\sqrt{A^2 + B^2} < 1$ .

## APPENDIX 2

Derivation of the Exact Phase Angle  $\theta_e$  for Equation (12)

Let the elementary solution be

$$\phi = e^{\alpha t} e^{i K_m x}. \quad (\text{A2.1})$$

One has

$$\phi_t = \alpha e^{\alpha t} e^{i K_m x}, \quad (\text{A2.2})$$

$$\phi_x = i K_m e^{\alpha t} e^{i K_m x}, \quad (\text{A2.3})$$

$$\phi_{xx} = -K_m^2 e^{\alpha t} e^{i K_m x}. \quad (\text{A2.4})$$

In the above,  $K_m$  ( $\equiv \frac{2\pi m}{2L}$ ,  $m = 0, 1, 2, 3, \dots, M$ ) denotes the wave number. As for  $2L$ , it is known as the period of the fundamental frequency ( $m = 1$ ). Substituting (A2.1)–(A2.4) into Eq. (12), we can derive  $\alpha$  as

$$\alpha = -(c + k K_m^2) - i u K_m. \quad (\text{A2.5})$$

As a result,  $\phi$  is expressed as

$$\phi = e^{-(c+kK_m^2+iuK_m)t} e^{i K_m x}. \quad (\text{A2.6})$$

By virtue of (A2.6), the amplification factor is exactly derived as

$$G_e = \frac{\phi(t + \Delta t)}{\phi(t)} = e^{-(c+kK_m^2+iuK_m)\Delta t}, \quad (\text{A2.7})$$

or

$$G_e = e^{i\theta_e} e^{-(c+kK_m^2)\Delta t}, \quad (\text{A2.8})$$

where

$$\theta_e = -u K_m \Delta t. \quad (\text{A2.9})$$

Invoking the definitions of  $\beta = K_m h$  and Courant number  $\nu = \frac{u \Delta t}{h}$  (where  $h$  is the grid size), we obtain the exact phase angle  $\theta_e$  as

$$\theta_e = -\beta \nu. \quad (\text{A2.10})$$

## ACKNOWLEDGMENTS

Financial support from the National Science Council of the Republic of China under Grant NSC88-2611-E-002-025 is acknowledged. The authors also acknowledge one of the reviewers who suggested referring to the exponential fitting method.

## REFERENCES

1. I. Harari and T. J. R. Hughes, Finite element methods for the Helmholtz equation in an exterior domain: Model problems, *Comput. Methods Appl. Mech. Eng.* **87**, 59 (1991).
2. F. Ilnca and D. Pelletier, Positivity preservation and adaptive solution for the  $k$ - $\epsilon$  model of turbulence, *AIAA J.* **36**(1), 44 (1998).
3. M. J. Crochet, A. R. Davies, and K. Walters, *Numerical Simulation of Non-Newtonian Flow* (Elsevier, New York, 1984).
4. L. Leboucher, Monotone scheme and boundary conditions for finite volume simulation of magnetohydraulic internal flows at high Hartmann number, *J. Comput. Phys.* **150**, 181 (1999).
5. B. Ataie-Ashtini, D. A. Lockington, and R. E. Volker, Numerical correction of finite difference solution of the advection–dispersion equation with reaction, *J. Contam. Hydrol.* **23**, 149 (1996).
6. M. A. Hossain, Modeling advective–dispersive transport with reaction: An accurate explicit finite difference model, *Appl. Math. Comput.* **102**, 101 (1999).
7. M. A. Hossain and D. R. Yonge, On Galerkin models for transport in groundwater, *Appl. Math. Comput.* **100**, 249 (1999).
8. I. Harari and T. J. R. Hughes, Stabilized finite element methods for steady advection–diffusion with production, *Comput. Methods Appl. Mech. Eng.* **115**, 165 (1994).
9. S. Idelsohn, N. Nigro, M. Storti, and G. Buscaglia, A Petrov–Galerkin formulation for advection–reaction–diffusion problems, *Comput. Methods Appl. Mech. Eng.* **136**, 27 (1996).
10. U. M. Ascher, Robert M. M. Mattheij, and Robert D. Russell, *Numerical Solution of Boundary Value Problems for Ordinary Differential Equations* (Prentice–Hall, Englewood Wood Cliffs, NJ, 1988).
11. E. P. Doolan, J. J. H. Miller, and W. H. A. Schilders, *Uniform Numerical Methods for Problems with Initial and Boundary Layers* (Boole Press, Dublin, 1980).
12. T. Tezdugar and Y. Park, Discontinuity capturing finite element formulations for nonlinear convection–diffusion–reaction equations, *Comput. Methods Appl. Mech. Eng.* **59**, 307 (1986).
13. R. Codina, A shock-capturing anisotropic diffusion for the finite element solution of the diffusion–convection–reaction equation, in *Finite Elements in Fluids, New Trends and Applications, Part 1*, edited by K. Morgan (Pineridge, Swansea, 1993), p. 67.
14. R. Codina, Comparison of some finite element methods for solving the diffusion–convection–reaction equation, *Comput. Methods Appl. Mech. Eng.* **156**, 185 (1998).
15. V. I. Poleyhaev, Numerical solution of the system of two-dimensional unsteady Navier–Stokes equations for a compressible gas in a closed region, *Fluid Dyn.* **2**, (1967).
16. R. F. Warming and B. J. Hyette, The modified equation approach to the stability and accuracy analysis of finite-difference methods, *J. Comput. Phys.* **14**, 159 (1974).
17. T. Meis and U. Marcowitz, *Numerical Solution of Partial Differential Equations*, Applied Mathematical Science Series, Vol. 22 (Springer-Verlag, Berlin/New York, 1981).
18. X. Yu, Finite difference methods for the reduced water wave equation, *Comput. Methods Appl. Mech. Eng.* **154**, 265 (1998).